Available online at www.sciencedirect.com
ScienceDirect
International Journal of Heat and Mass Transfer 51 (2008) 2109–2122
International Journal of HEAT and MASS TRANSFER
www.elsevier.com/locate/ijhmt

Rapid microfluidic thermal cycler for polymerase chain reaction nucleic acid amplification

Shadi Mahjoob [a], Kambiz Vafai [a,*], N. Reginald Beer [b]

[a] *Mechanical Engineering Department, University of California, Riverside, CA 92521, USA*
[b] *Lawrence Livermore National Laboratory, Center for Micro and Nanotechnology, USA*

Received 15 September 2007; received in revised form 3 November 2007
Available online 29 January 2008

Abstract

Polymerase chain reaction (PCR) is widely used in biochemical analysis to amplify DNA and RNA in vitro. The PCR process is highly temperature sensitive, and thermal management has an important role in PCR operation in reaching the required temperature set points at each step of the process. The goal of this research is to achieve a thermal technique to rapidly increase the heating/cooling thermal cycling speed while maintaining a uniform temperature distribution throughout the substrate containing the aqueous nucleic acid sample. In this work, an innovative microfluidic PCR thermal cycler, which utilizes a properly arranged configuration filled with a porous medium, is investigated. Various effective parameters that are relevant in optimizing this flexible heat exchanger are investigated such as heat exchanger geometry, flow rate, conductive plate, the porous matrix material, and utilization of thermal grease. An optimized case is established based on the effects of the cited parameters on the temperature distribution and the required power for circulating the fluid in the heat exchanger. The results indicate that the heating/cooling temperature ramp of the proposed PCR heat exchanger is considerably higher (150.82 °C/s) than those in the literature. In addition, the proposed PCR offers a very uniform temperature in the substrate while utilizing a low power.

1. Introduction

The polymerase chain reaction (PCR) is the most commonly used molecular biology technique for DNA amplification in vitro. This technique has a variety of applications such as paternity testing, generic fingerprinting, mutagenesis, analysis of ancient DNA, cloning genes, detection of hereditary diseases, genotyping of specific mutations, comparison of gene expression, and viral or bacterial pathogen detection. This technique consists of three steps of denaturing, annealing, and elongation, respectively. In the first step, the DNA template is heated up to the denaturation temperature (approximately 96 °C) and will be heated for 20–30 s to separate the DNA double strands. In the second step, annealing, the temperature of the DNA decreases to the annealing temperature (approximately 50–65 °C, depending on the primer length and percent guanine and cytosine content) and will be kept at this temperature for 20–40 s so that the primers can anneal to the single stranded DNA template through Brownian motion in the solution and subsequent hydrogen-bonding [1]. In the third step, elongation or extension, the DNA temperature is increased to the elongation temperature (approximately 72 °C) to synthesize new DNA strands complementary to the DNA template strands. The elongation time depends on the DNA polymerase used and on the length of the DNA fragment to be amplified, and it can vary from a few seconds to few minutes. After each three-step cycle, every DNA is doubled and so after n cycles, the DNA template is amplified to 2^n similar DNA. At the first cycle, as an initialization step, the PCR reaction is often heated at the denaturation temperature for a specified time to activate the DNA polymerase, after which the thermal cycling

* Corresponding author. Tel.: +1 9518272135; fax: +1 9518272899.
E-mail address: vafai@engr.ucr.edu (K. Vafai).

0017-9310/$ - see front matter © 2007 Elsevier Ltd. All rights reserved.
doi:10.1016/j.ijheatmasstransfer.2007.11.014

Nomenclature

c	specific heat
d_p	particle diameter
Da	Darcy number
F	geometric function
h	convective heat transfer coefficient
k	thermal conductivity
k_{eff}	effective thermal conductivity
K	permeability
P	pressure
q	heat flux
t	time
t_{cp}	conductive plate thickness
t_e	exit channel thickness
t_i	inlet channel thickness
t_p	porous matrix thickness
$t_{p,Max}$	maximum porous matrix thickness
T	temperature
u	velocity
$\vec{v}$	velocity vector
x	horizontal coordinate
X	dimensionless horizontal coordinate
y	vertical coordinate

Greek symbols

ε	porosity
ρ	density
μ	dynamic viscosity
υ	kinematic viscosity
Λ	inertia parameter

Subscripts

f	fluid
s	solid
b	bulk flow
w	wall

Symbol

$\langle\ \rangle$	"Local volume average" of a quantity

begins. Also at the end of the last cycle, as a final elongation step, the template may be heated at the elongation temperature for few minutes.

The PCR process should be completed as fast as possible since the time decreases the activity of Taq DNA polymerase [2]. Slower or inaccurate temperature transition from the denaturation step to the annealing step increases the chance of primer–dimer formation which is the bonding of the primers (forward and reverse) to each other, or to other primers in the multiplexed reaction. It also increases the chance of nonspecific amplification which is bonding of the primers to sequences in the DNA template that are not exactly complimentary to the primer [1]. Quick cycles can be achieved by decreasing PCR dwell times. This can be achieved using rapid thermal cyclers. As such, thermal management has an important role in reaching the required temperature rapidly while maintaining a uniform temperature distribution along the substrate channel where the DNA template is placed.

In the initial PCR systems, heated water baths were used to achieve the necessary temperature cycles. Presently, one method for conventional PCR machines to control the temperature in the micro-centrifuge reaction tubes is by utilizing Peltier elements, which are mounted on a metal block. Cycling is achieved by heating and cooling the massive metal block with a maximum temperature ramp of 1–3 °C/s. In fact, to ensure temperature homogeneity across the whole plate, a large value of thermal capacitance of the system is required, resulting in slow PCR cycles. In these machines, every cycle usually takes 4 min and it takes around 2 h to perform the full PCR process. These machines accommodate a number of parallel reactions with typical volumes of 10–100 μL [3]. Excessive reaction volume, high power consumption and low efficiency are some of the barriers in the application of PCR [4].

Utilizing smaller instruments and reduced reaction volumes can result in faster cycles. The miniaturized DNA reaction chambers have advantages in integration, process speed, efficiency, and decrease in the consumption of expensive reaction materials. The first miniaturized PCR appeared in 1993 [5] with simple micromachined chemical reactors with integrated heaters for PCR in Lawrence Livermore National Lab [3]. Swerdlow et al. [6] studied PCR in thin fluidic capillary tubes and used air forced convection for thermal management. They reported that they could decrease the PCR cycle time from 1 to 4 h (which is in conventional machines) to 20 min. Huhmer and Landers [7] studied the PCR for the sample in thin glass capillary tube using Tungsten lamp for heating and utilized air forced convection for cooling thermal management. They reported 65 °C/s and 20 °C/s for heating and cooling, respectively. Lee et al. [1] used infrared (IR) heating and water impingement cooling technique for PCR in thin glass capillary tubes. They reported a temperature rate of 65 °C/s and 80 °C/s for heating and cooling processes. They also studied two other cooling methods, natural convection and air forced convection, which performed 2 °C/s and 6 °C/s temperature ramps, respectively.

Utilizing a broad range of microfabrication technologies and materials, miniaturized chips made of silicon, glass, or polymeric materials such as PDMS (polydimethylsiloxane) are being used to improve PCR efficiency [8–18]. PDMS is the most widely used silicon-based organic polymer. In some of the PCR microchips, continuous flow system is used. In these devices, the DNA sample is subjected to flow

at three constant temperature zones for three PCR steps [19–23].

Khandurina et al. [24] utilized a compact thermal cycling assembly based on dual Peltier thermoelectric elements coupled with a microchip gel electrophoresis platform for a PCR microchip. They reported temperature ramps of 2 °C/s for heating and 3–4 °C/s for cooling. Lagally et al. [25] used an integrated microfluidic device which consists of submicroliter PCR chambers etched into a glass substrate. They used nitrogen flowing over the top of the chip for cooling and thin film heaters and reported cooling/heating rates of around 10 °C/s. A similar thermal management is used in Ref. [26]. In another study by Lagally et al. [27], the authors improved the heating/cooling temperature ramps to 20 °C/s utilizing an integrated PCR-CE device including micro-fabricated heaters and resistance temperature detectors (RTDs) within the PCR chambers.

Niu et al. [4] used a PDMS-glass hybrid micro PCR chip and zigzag shaped Pt heater for heating and a fan for forced convection cooling. They reported 10 °C/s and 4.6 °C/s as heating and cooling temperature ramps of the sample. For DNA amplification, a PDMS-silicon chip was designed and optimized by Bhattacharya et al. [28]. The thermal management is done by a current controller with a power MOSFET serving as a pulse width modulation device by varying the duty cycle of the gate voltage as a switch. The heating and cooling temperate ramps are reduced by a factor of ten from the conventional thermal cycling machines.

Although materials such as glass or polymers are currently popular for bioanalysis in pipetted systems, silicon has some advantages. Glass-based devices have good thermal conductivity, while the conductivity of silicon is excellent. In combination with thin film heaters and temperature sensors, precise temperature control of silicon devices is possible. Due to the existence of the semiconductor industry, micro chambers can be easily fabricated in silicon and the shape can be precisely controlled with photolithography and etching technology. Silicon can be combined with thin film technology for implementing sensors [29]. Daniel et al. [29] utilized a silicon micro-chip etching with a thermal design of the PCR chambers, combined with thin film platinum resistors as temperature sensors and heaters. They reported a cooling temperature rate of 74 °C/s and a heating rate of 60–90 °C/s which actually depends on the available input power. Silicon-based thermo-cyclers have been studied by Poser et al. [30]. They utilized a thin film heater and a fan for forced convection cooling and reported 80 °C/s and 40 °C/s temperature rates. Yoon et al. [2] fabricated silicon based PCR chips and utilized platinum thin film micro heater. They obtained 36 °C/s and 22 °C/s for heating and cooling rates. Hofmann et al. [3] developed a miniaturized silicon based PCR chip and utilized a miniaturized resistor-based platinum heater fabricated on a Pyrex substrate. In a recent study, the PCR system was made of silicon micro-machined into the shape of a cantilever terminated with a disc [31]. Thermal management was done by a thin film heater.

In this work, an innovative PCR heat exchanger (Fig. 1), utilizing porous inserts, is proposed and various pertinent parameters on its performance are investigated, such as heat exchanger geometry (exit and inlet channel thickness, exit channel location, inclination angle, maximum porous matrix thickness, and conductive plate thickness), the properties of the plate and porous matrix solid parts, the heating/cooling fluid velocity and flow rate, and utilization of thermal grease (Tables 1 and 2). Porous inserts are attractive choices in heat transfer augmentation. They provide a very large surface area for a given volume which is a key parameter in heat transfer processes. Vafai et al. have demonstrated the advantages of porous inserts in variety of thermal transport issues such as external heat transfer enhancement [32], regulating skin friction and enhancing heat transfer rate over intermittently emplaced porous cavities [33], biological tissue modeling [34,35], thin films [36], isothermal surface [37], and disk shaped and flat plate heat

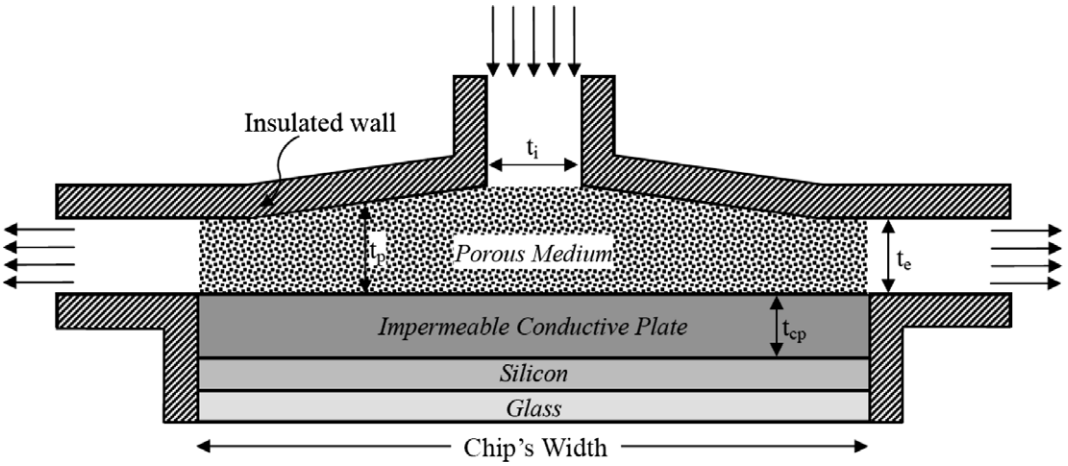

Fig. 1. Schematic of physical model of PCR heat exchanger along with the silicon–glass PCR microchip.

Table 1
Investigated optimization parameters

Studied parameter	Case ID	Geometry
	Case A (base case)	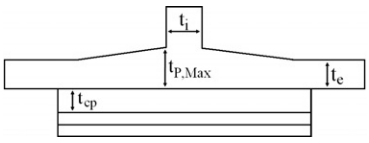
Exit channel thickness	Cases B and C	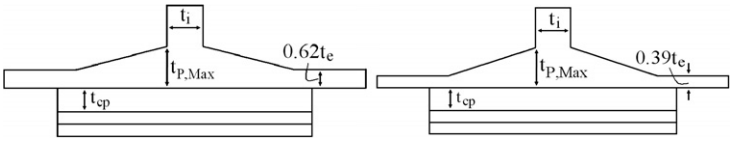
Exit channel configuration	Case D	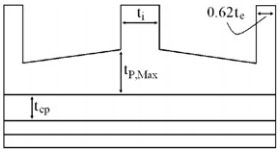
Inlet channel thickness and flow rate	Cases E and F	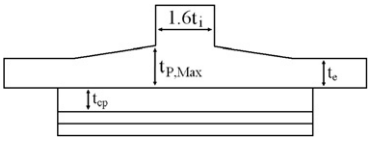
Heating/cooling fluid velocity	Cases G and H	The geometry is the same as that of the base case
Solid material	Cases I and J	The geometry is the same as that of the base case
Conductive plate thickness	Case K	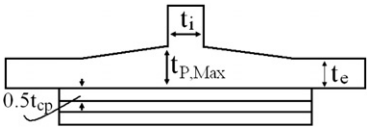
Utilizing thermal grease	Cases L, M, N,O	The geometry is the same as that of the base case
	Case P (optimized case)	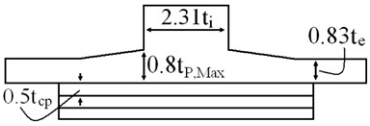

pipes [38,39]. Competing technologies such as jet impingement and micro-channel cooling [40,41] were also considered in selecting the current setup.

The PCR thermal cycling performance is specified by temperature ramp, temperature uniformity along the substrate, and the required power. In earlier investigations, only some of theses performance factors were considered or presented. In this work, an optimized heat exchanger is presented based on a comprehensive investigation. The heating/cooling temperature ramps of this heat exchanger are considerably higher than those in the literature. The proposed device can produce a very uniform temperature along the substrate where the DNA channel is placed while utilizing a low input power.

2. PCR set-up

In this work, a heating/cooling microscale thermocycler, attached to a PCR micro-chip, is investigated. The chip is composed of a silicon substrate and a glass layer. The glass is used for visualization and the DNA channel will be etched in the silicon layer close to the silicon–glass interface. The cross-sectional view of the physical model of the heat exchanger, along with the PCR chip, is presented in Fig. 1. Typical dimensions for these chips are 59.5 mm length, 10.5 mm width, and 1 mm thickness (0.5 mm for each layer).

The heat exchanger consists of inlet and exit channels where heating/cooling fluid is passing through, an enclo-

Table 2
Different case studies[a]

Studied parameter	Case ID	Exit channel thickness		Inlet channel thickness		Maximum thickness of porous matrix		Velocity		Flow rate		Plate thickness		Solid material
		Normalized thickness	**Relative to the base case (A)**	Normalized thickness	**Relative to the base case (A)**	Normalized thickness	**Relative to the base case (A)**	Value (m/s)	**Relative to the base case (A)**	Value $\times 10^3$ (m^3/s)	**Relative to the base case (A)**	Normalized thickness	**Relative to the base case (A)**	
	A	0.114	**1**	0.143	**1**	0.162	**1**	2.2	**1**	0.196	**1**	0.095	**1**	Copper
Exit channel thickness	B	0.071	**0.623**	0.143	**1**	0.162	**1**	2.2	**1**	0.196	**1**	0.095	**1**	Copper
	C	0.045	**0.395**	0.143	**1**	0.162	**1**	2.2	**1**	0.196	**1**	0.095	**1**	Copper
Exit channel configuration	D	0.071	**0.623**	0.143	**1**	0.162	**1**	2.2	**1**	0.196	**1**	0.095	**1**	Copper
Inlet channel thickness and flow rate	E	0.114	**1**	0.229	**1.6**	0.162	**1**	2.2	**1**	0.314	**1.6**	0.095	**1**	Copper
	F	0.114	**1**	0.229	**1.6**	0.162	**1**	1.375	**0.625**	0.196	**1**	0.095	**1**	Copper
Heating/cooling fluid velocity	G	0.114	**1**	0.143	**1**	0.162	**1**	1.375	**0.625**	0.123	**0.625**	0.095	**1**	Copper
	H	0.114	**1**	0.143	**1**	0.162	**1**	3.52	**1.6**	0.314	**1.6**	0.095	**1**	Copper
Solid material	I	0.114	**1**	0.143	**1**	0.162	**1**	2.2	**1**	0.196	**1**	0.095	**1**	Gold
	J	0.114	**1**	0.143	**1**	0.162	**1**	2.2	**1**	0.196	**1**	0.095	**1**	Silver
Conductive plate thickness	K	0.114	**1**	0.143	**1**	0.162	**1**	2.2	**1**	0.196	**1**	0.048	**0.5**	Copper
Utilizing thermal grease														
Silver grease, thickness: 3 μm	L	0.114	**1**	0.143	**1**	0.162	**1**	2.2	**1**	0.196	**1**	0.095	**1**	Copper
Silicon grease, thickness: 3 μm	M	0.114	**1**	0.143	**1**	0.162	**1**	2.2	**1**	0.196	**1**	0.095	**1**	Copper
Silver grease, thickness: 30 μm	N	0.114	**1**	0.143	**1**	0.162	**1**	2.2	**1**	0.196	**1**	0.095	**1**	Copper
Silver grease, thickness: 300 μm	O	0.114	**1**	0.143	**1**	0.162	**1**	2.2	**1**	0.196	**1**	0.095	**1**	Copper
	P	0.095	**0.833**	0.33	**2.308**	0.130	**0.802**	0.6	**0.273**	0.125	**0.638**	0.048	**0.5**	Copper

[a] All thicknesses are normalized by chip's width.

sure, and a layer of conductive plate which will be attached to the PCR micro-chip. The enclosure is filled with a conductive porous medium of uniform porosity and permeability. The nominal permeability and porosity of the porous matrix are taken as $3.74 \times 10^{-10}\,\mathrm{m}^2$ and 0.45, respectively. The porous medium is saturated with heating/cooling fluid coming through an inlet channel. The inlet channel will be connected to hot and cold supply tanks. A switching valve is used to switch between hot and cold tanks for heating and cooling cycles. All lateral walls and top of the porous medium are insulated to minimize losses.

The thermal cycling processes are as follows: first in a heating cycle, the temperature is increased to the denaturation temperature very quickly by inserting hot fluid through the inlet channel to start the first PCR step. The system will be kept at that temperature for a specified time by passing the hot fluid with denaturation temperature continuously to avoid any temperature change in the chip. Then the switching valve is used to pass cooling fluid through the heat exchanger at the annealing temperature to cool the substrate very quickly to the annealing temperature. The cooling fluid at annealing temperature moves through the system until the second PCR step is completed. Finally, the hot fluid at elongation temperature enters the system to raise the chip temperature to the elongation temperature very quickly. The hot fluid moves in the system until the third PCR step is also completed and a PCR cycle is completed. This heating/cooling cycling continues until the desired DNA amplification is achieved.

3. Governing equations

Three different regions need to be analyzed for the proposed system. These are, the inlet and exit channels, the porous substrate, and the solid layers:

3.1. Inlet/exit channels

The governing equations representing transient, single phase, incompressible flow inside the inlet/exit channels are

$$\nabla \cdot \vec{v} = 0 \tag{1}$$

$$\rho_f \frac{\partial}{\partial t}(\vec{v}) + \rho_f \vec{v} \cdot \nabla \vec{v} = -\nabla p + \mu \nabla^2 \vec{v} \tag{2}$$

$$\rho_f c_f \frac{\partial T}{\partial t} + \rho_f c_f (\vec{v} \cdot \nabla T) = k_f \nabla^2 T \tag{3}$$

3.2. Porous substrate

For the porous medium, the transient, single phase volume averaged continuity, momentum, and energy equations are [42]

$$\nabla \cdot \langle \vec{v} \rangle = 0 \tag{4}$$

$$\frac{\rho_f}{\varepsilon}\left[\frac{\partial}{\partial t}\langle \vec{v} \rangle + \langle (\vec{v} \cdot \nabla)\vec{v} \rangle\right] = -\nabla \langle p \rangle^f + \frac{\mu}{\varepsilon}\nabla^2 \langle \vec{v} \rangle - \frac{\mu}{K}\langle \vec{v} \rangle - \frac{\rho_f F \varepsilon}{\sqrt{K}}[\langle \vec{v} \rangle \cdot \langle \vec{v} \rangle]J \tag{5}$$

$$\frac{\partial}{\partial t}(\varepsilon \rho_f c_f \langle T \rangle + (1-\varepsilon)\rho_s c_s \langle T \rangle) + \rho_f c_f \langle \vec{v} \rangle \cdot \nabla \langle T \rangle = k_{eff} \nabla^2 \langle T \rangle \tag{6}$$

where,

$$k_{eff} = \varepsilon k_f + (1-\varepsilon) k_s \tag{7}$$

$$F = \frac{1.75}{\sqrt{150\varepsilon^3}} \tag{8}$$

$$K = \frac{\varepsilon^3 d_p^2}{150(1-\varepsilon)^2} \tag{9}$$

3.3. Solid layers

For each solid layer of the setup, i.e. the conductive plate and the silicon and glass, the energy equation is

$$\rho_s c_s \frac{\partial T}{\partial t} = k_s \nabla^2 T \tag{10}$$

The heating/cooling fluid is liquid water with constant properties. In order to study the heating/cooling temperature ramps, the temperature of the hot fluid is taken as 96 °C and the temperature of the cold fluid is taken as 50 °C.

4. Computational methodology

An implicit, pressure-based, cell-centered finite volume method is used to solve the highly coupled and nonlinear governing equations. As such, the governing equations are discretized and linearized for each cell of the computational grid spatially and temporally. For spatial discretization of the convection terms, second order upwind method is used and for the diffusion terms central differencing is applied. The temporal discretization is done implicitly with a very small time step of 10^{-5} s. Resulting algebraic equations are solved using Gauss–Seidel point implicit linear equation solver in conjunction with an algebraic multi-grid (AMG) method in order to reduce the dispersion errors along with increasing the speed of the computations [43]. The governing equations are solved sequentially. For this purpose, at each time step, first the momentum equations are solved to obtain the velocity field. Next, the continuity equation is solved utilizing the SIMPLE algorithm for pressure–velocity coupling to obtain and modify the pressure field, mass fluxes, and velocity field. Finally, the energy equation is solved to obtain the temperature field. An iterative procedure utilizing under-relaxation is used. Convergence is assumed when residuals become less than 10^{-6}. First, the steady state forms of the governing equa-

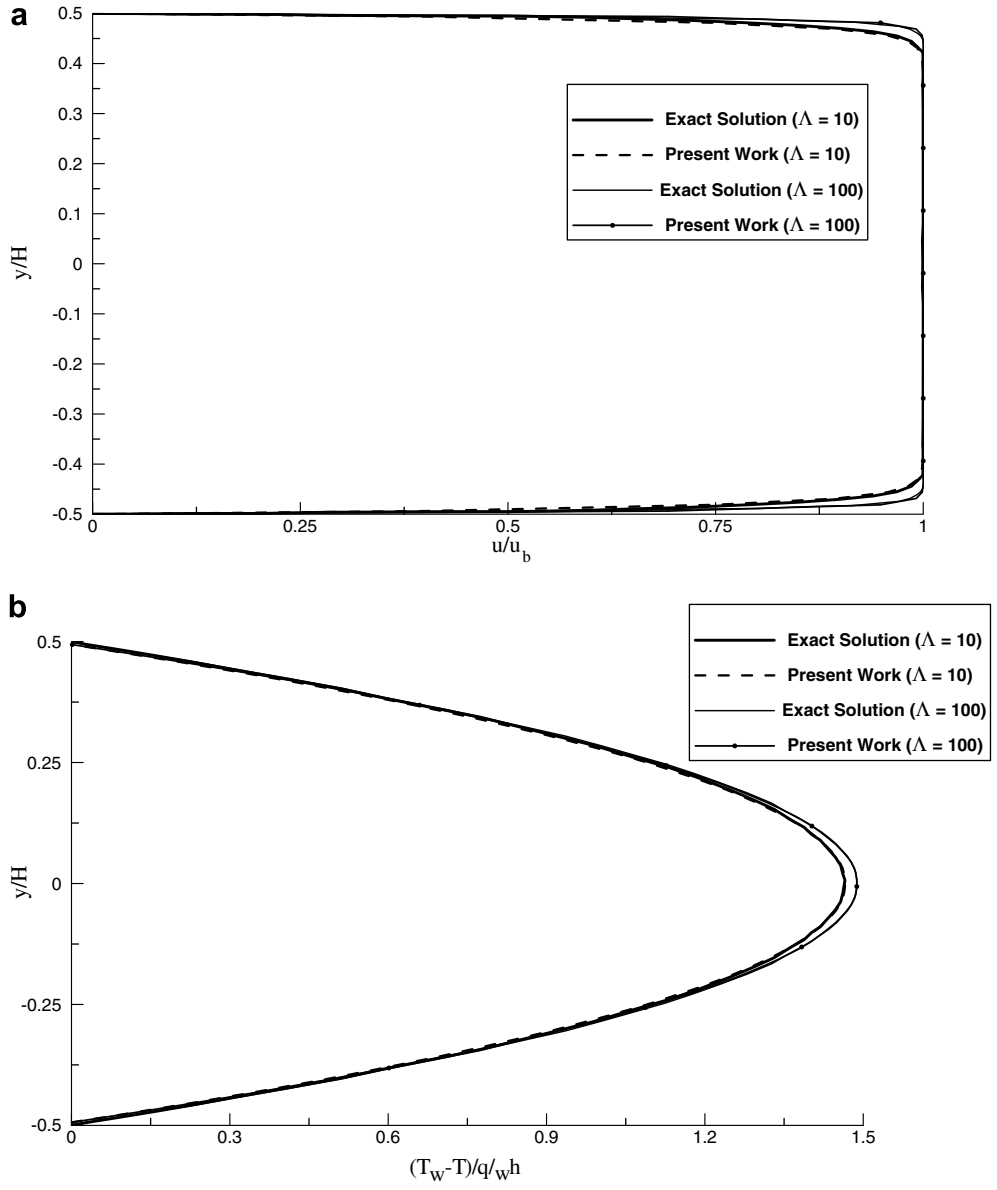

Fig. 2. Comparison of the present work with an exact solution [44] at the midsection of a channel filled with a porous medium (a) dimensionless velocity profile at $Da^{-1/2} = 30$, $\Lambda = 10{,}100$ (b) dimensionless temperature profile at $Da^{-1/2} = 30$, $\Lambda = 10$, 100.

tions are solved. The steady state solution is then used as an initial input for the transient form of the governing equations.

4.1. Code validation

To validate the numerical results, they are compared to an exact solution given by Vafai and Kim [44] for different inertia parameters (Λ) with the Darcy number of 10^{-3}, that is

$$\Lambda = \varepsilon^{3/2} F \frac{u_b H}{\upsilon_f} \tag{11}$$

$$Da = \frac{1}{H^2}\frac{K}{\varepsilon} \tag{12}$$

where $2H$ indicates the channel height. Obtained normalized velocity and temperature profiles at the midsection of the channel are compared with that of an exact solution [44]. The comparison indicates an excellent agreement for velocity and temperature profiles for different inertia parameters (Fig. 2).

4.2. Computational grid resolution study

A multi-block and structure grid is utilized for grid generations. In order to study grid independency of the results, several grid distributions were investigated by comparing temperature and velocity fields at various time steps. As an example, the temperature profile for different grid resolutions are presented at the silicon–glass interface, which is

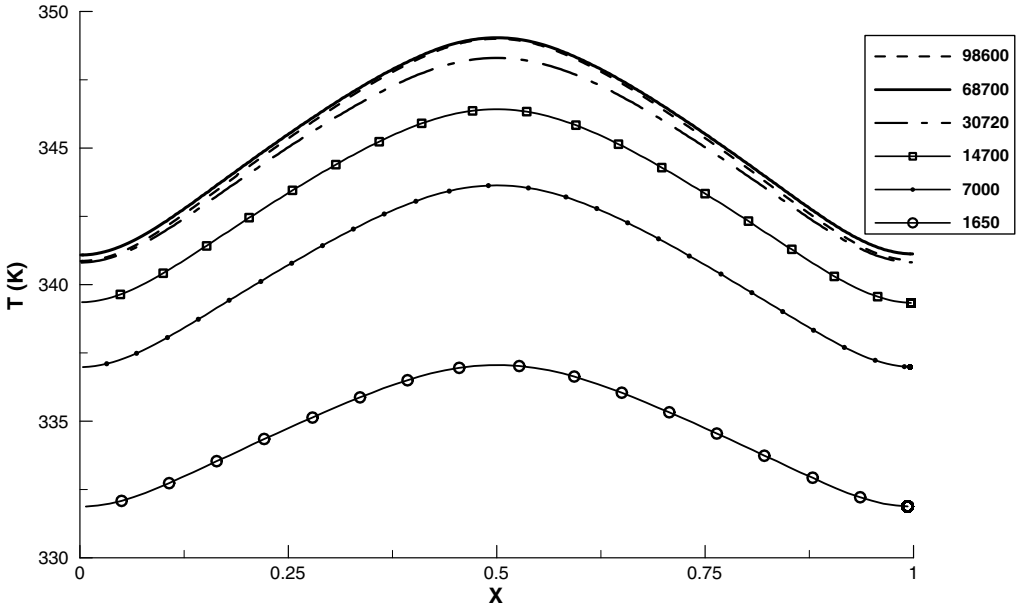

Fig. 3. Temperature profile at the silicon–glass interface for grid independence study.

the major parameter for design of the heat exchanger (Fig. 3). Our grid independence study indicates that a gird resolution composed of 68,700 cells results in a grid independent solution.

5. Results

The PCR system is investigated based on the cycling time, uniformity of temperature at silicon–glass interface, and the required power to overcome the pressure drop in the system (Table 3). The cycling time is the required time for the silicon–glass interface to reach the new steady temperature with a maximum deviation of 0.25 °C. Temperature change per second, so called temperature ramp, is the temperature change per cycling time. One of the effective parameters to optimize the heat exchanger is the inclination angle, i.e. the angle of the top surface of the porous media with respect to the horizontal line. This angle also

Table 3
Pressure drop, required pumping power, cycle time and temperature ramp for each case

Studied parameter	Case ID	Pressure drop		Required pumping power		Cycling time (s)	Temperature ramp	
		Value (kPa)	**Relative to the base case (A)**	Value (W)	**Relative to the base case (A)**		Value (°C/s)	**Relative to the base case (A)**
	A	234	**1**	45.86	**1**	0.335	137.3	**1**
Exit channel thickness	B	381	**1.628**	74.68	**1.628**	0.335	137.3	**1**
	C	673	**2.876**	131.91	**2.876**	0.325	141.54	**1.031**
Exit channel configuration	D	264	**1.128**	51.74	**1.128**	0.35	131.43	**0.957**
Inlet channel thickness and flow rate	E	481	**2.056**	151.03	**3.293**	0.315	146.03	**1.063**
	F	194	**0.829**	38.02	**0.829**	0.33	139.4	**1.015**
Heating/cooling fluid Velocity	G	96	**0.410**	11.81	**0.257**	0.355	129.58	**0.944**
	H	582	**2.487**	182.75	**3.985**	0.33	139.4	**1.015**
Solid material	I	234	**1**	45.86	**1**	0.36	127.8	**0.931**
	J	234	**1**	45.86	**1**	0.325	141.54	**1.031**
Conductive plate thickness	K	234	**1**	45.86	**1**	0.305	150.82	**1.098**
Utilizing thermal grease	L	234	**1**	45.86	**1**	0.345	133.3	**0.971**
	M	234	**1**	45.86	**1**	0.38	121.05	**0.882**
	N	234	**1**	45.86	**1**	0.375	122.7	**0.89**
	O	234	**1**	45.86	**1**	0.665	69.2	**0.504**
	P	98.9	**0.423**	12.36	**0.269**	0.305	150.82	**1.098**

affects the exit channel or inlet channel thicknesses. Other effective parameters are the location of the exit channel, maximum porous matrix thickness, heating/cooling flow rate and velocity, the material utilized in constructing the porous matrix and the conductive plate.

5.1. Heating/cooling PCR cycling

In Fig. 4, temperature distribution, at different times, along the silicon–glass interface for the base case (A) is presented at different times in heating and cooling cycles. The heating cycle increases the temperature from 323 K to 369 K rapidly, in 0.335 s (Fig. 4a). The same temperature ramp is achieved in the cooling cycle, from 369 K to 323K (Fig. 4b). The heating/cooling cycling times are considerably short in comparison with those cited in the literature. The main temperature change occurs in the first 0.1 s (Fig. 5). At $t = 0.1$ s, the temperature at the interface is around 366.5 K (in the heating cycle) and 325.5 K (in the cooling cycle), only 2.5 °C different from the required temperature. In addition, a very uniform temperature exists at the interface after $t = 0.05$ s (Fig. 4). As such, in what follows $t = 0.02$ s is selected to demonstrate the effects of different parameters on the highest temperature distribution

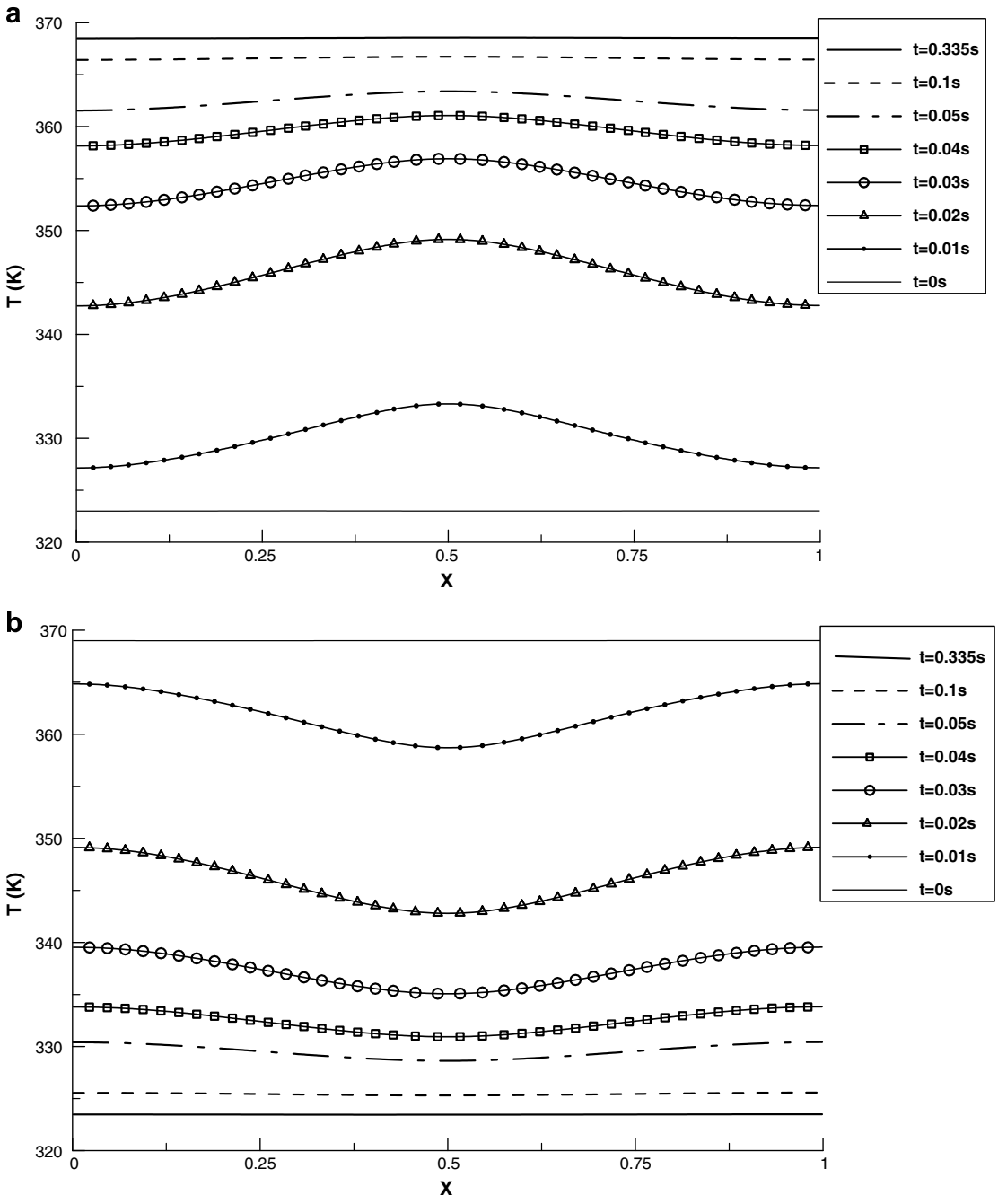

Fig. 4. Temporal temperature distribution at the silicon–glass interface for the base case in (a) heating cycle (b) cooling cycle.

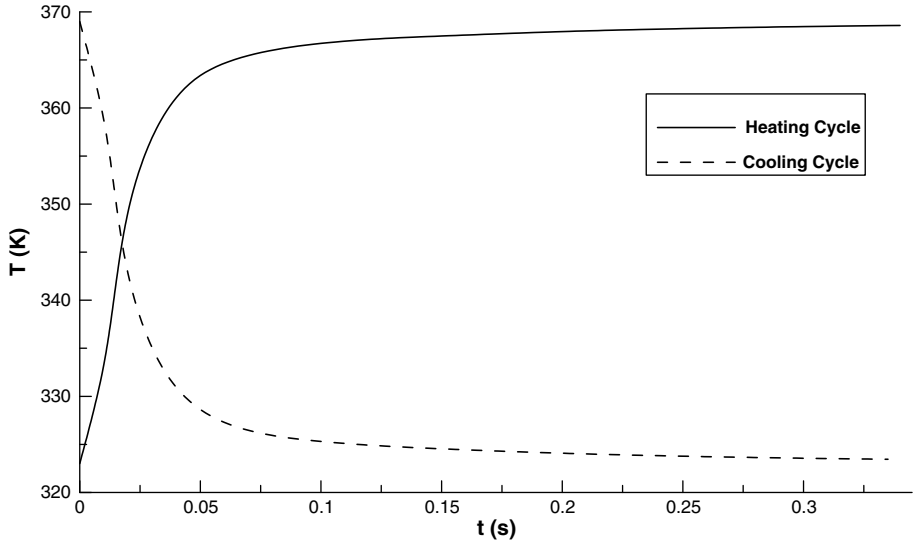

Fig. 5. Temporal variation of temperature at the center point of the silicon–glass interface for the base case in heating and cooling cycles.

non-uniformity. At these rates, adding a short pause at the elongation temperature of 345 K to allow the polymerase time to extend the entire amplicon, may be required for long amplification sequences (At 72 °C the enzyme adds bases at approximately 100 bp per second).

5.2. Effects of exit channel thickness

As seen in Fig. 6 and Table 3, decreasing the exit channel thickness, i.e. from case A to case C, improves the cycling speed and the temperature ramp. In addition, a decrease in the thickness of the exit channel results in a more uniform temperature along the silicon–glass interface. This is because the hot/cold fluid is being forced to pass closer to the wall resulting in a more effective heat transfer with the conductive plate and the silicon–glass interface. However, decreasing the exit channel thickness increases the pressure drop (Table 3) since the inclination angle has been increased resulting in larger surface area change, in the flow direction.

5.3. Effects of the exit channel location

The effect of the exit channel location is presented in Fig. 6. Cases A and D, horizontal and vertical exits, respectively, have exactly the same porous medium cross-section. As can be seen, for the vertical exit case, heat transfer is reduced at the corners of the porous medium over the conductive plate due to the velocity distribution (Fig. 7a). For the horizontal exit case, the hot/cold fluid can pass the por-

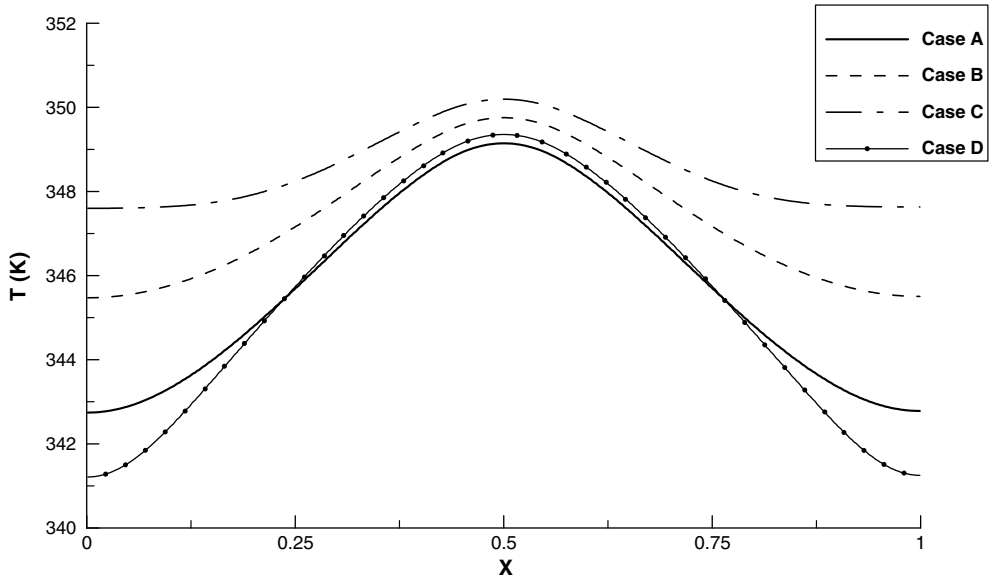

Fig. 6. The effects of exit channel thickness and location on the temperature distribution at the silicon–glass interface at $t = 0.02$ s.

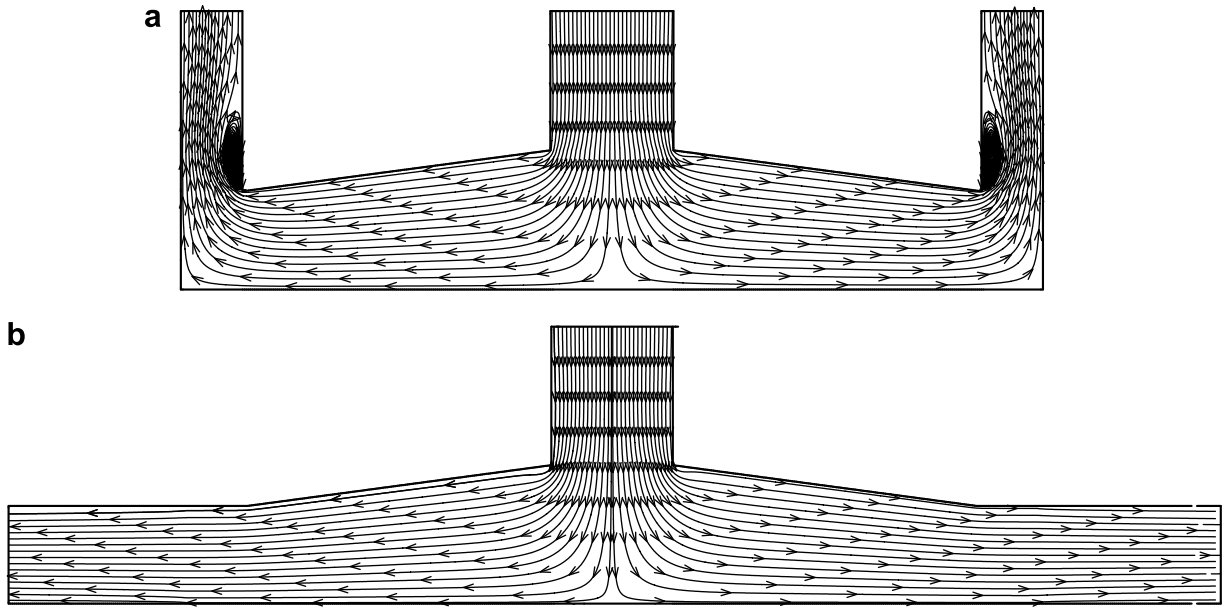

Fig. 7. The effect of exit channel position on the streamlines through the medium (a) vertical exit channel (case D) (b) horizontal exit channel (case A).

ous medium parallel to the wall resulting in a more uniform temperature along the interface of the porous medium and the conductive plate (Fig. 7b). The larger non-uniformity in temperature for the vertical exit case results in a longer cycle (Table 3). In addition, changing the exit channel location from lateral to vertical increases the pressure drop (Table 3).

5.4. Effects of inlet channel thickness and fluid flow rate

The effects of the inlet channel thickness are shown in Fig. 8. The figure shows that increasing the inlet channel thickness (from case A to case E) has maintained a more uniform temperature along the silicon–glass interface while increasing the temperature ramp significantly (Table 3). However, increasing the thickness increases the flow rate, resulting in considerably higher pressure drop in the system. To check the effects of changing the thickness itself, case F which has the same flow rate as case A but posses a larger inlet thickness (similar to case E) is investigated. Fig. 8 and Table 3 demonstrate that at constant flow rate, increasing the inlet channel thickness results in a more uniform temperature and a reduction with required power.

5.5. Effects of the heating/cooling fluid velocity

Fig. 8 also displays the effects of the fluid velocity on the silicon–glass interface temperature distribution. It can be

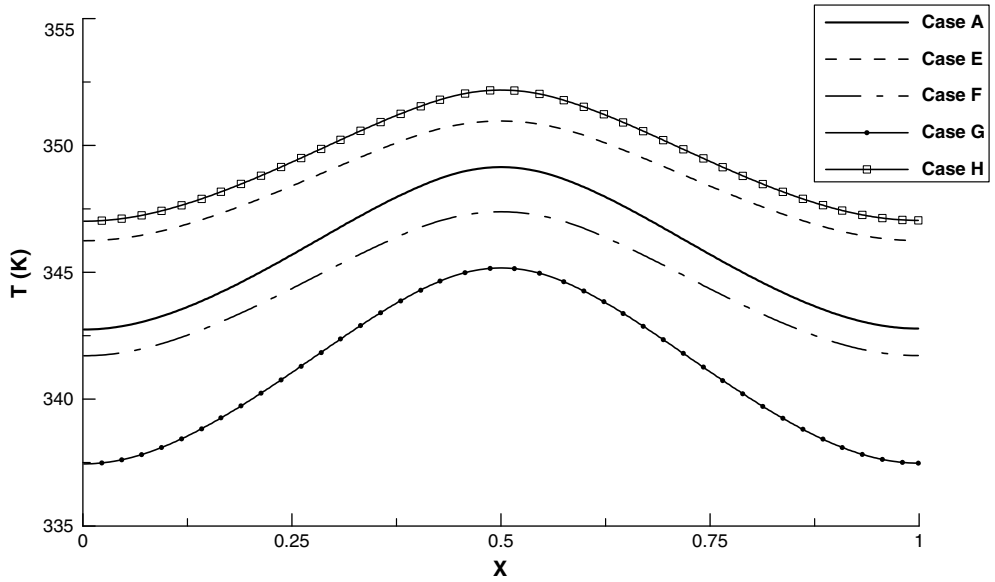

Fig. 8. The effects of inlet channel thickness, flow rate and fluid velocity on the temperature distribution at the silicon–glass interface at $t = 0.02$ s.

seen that increasing the fluid velocity can increase the cycling speed while maintaining a more uniform temperature distribution. The figure indicates, although the velocity increase from case G to case A is the same as that from case A to case H (1.6 times), the cycling speed increases faster at lower fluid velocities. Further an increase in the fluid velocity increases the pressure drop (Table 3). Therefore, there exists an optimum fluid velocity for an optimized cycling time. Comparing cases of F and G, and also A and E, which have the same velocity but different inlet thickness (different inclination angles) indicates that increasing the inlet channel thickness at constant velocity can result in faster cycling, more uniform temperature and a larger pressure drop.

5.6. Effects of the conductive plate

Fig. 9 shows the effect of different solid materials (copper, gold and silver) utilized for the conductive plate and the porous matrix on the temperature profile of silicon–glass interface (cases A, I, and J). The figure indicates that silver and gold produce only a slightly more uniform temperature distribution than the copper. Silver can reduce the thermal cycling time but again only slightly. Therefore, considering the cost of using silver in comparison with that of copper, the latter is a more viable choice for the heat exchanger. As it is expected the pressure drop does not change when utilizing different solid materials (Table 3).

Also, seen in Fig. 9, decreasing the thickness of the conductive plate to half the base case (case K) increases the cycle speed considerably resulting in a temperature ramp increase from 137.3 to 150.82 °C/s (Table 3). Our investigation indicates the existence of an optimum thickness.

5.7. Effects of utilizing thermal grease

In composite solid systems, a temperature drop occurs across the interface between solid layers due to the surface roughness of the solids. Thermal grease is used in the gaps to improve the thermal heat conductance at the interface between two adjacent solids. There are many types of thermal grease, such as silicon based, ceramic based and metal based thermal grease. The silicon based thermal grease is usually white and has a moderate thermal conductivity. The ceramic-based thermal grease contains ceramic particles suspended in other thermally conductive ingredients. It conducts heat better than most silicon greases. The metal-based thermal grease contains metal particles (usually silver) and other conductive ingredients. Metal thermal grease has a better thermal conductivity than the other types. Two nominal thermal greases were considered in this work: silver grease (cases L, N, O) with the thermal conductivity of 10 W/mK and silicon grease (case M) with the thermal conductivity of 0.9 W/mK. It is assumed that the grease fills a layer between the conductive plate and the silicon layer of the chip. The nominal thickness of the grease layer was varied from 3×10^{-3} mm to 300×10^{-3} mm, based on the maximum roughness of the copper/silicon solid materials as well as tolerance stackup in the device/conductive plate assembly. Incorporating the thermal resistance resulting from the use of thermal grease has an insignificant effect on the temperature distribution uniformity (Fig. 10) and it has a small effect on the thermal cycling speed when the silver grease is used (Table 3). Investigating the exaggerated thicknesses (30×10^{-3} mm and 300×10^{-3} mm) to account for the worse case manufacturing scenarios indicates that even with the grease thickness of one or two orders of magnitude larger than

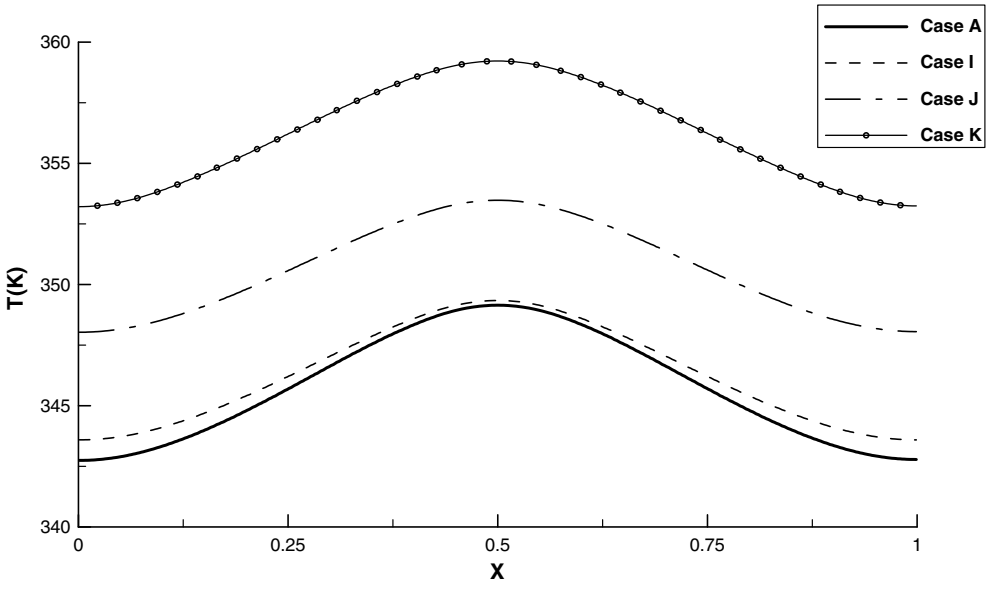

Fig. 9. The effects of solid material and the thickness of the conductive plate on the temperature distribution at the silicon–glass interface at $t = 0.02$ s.

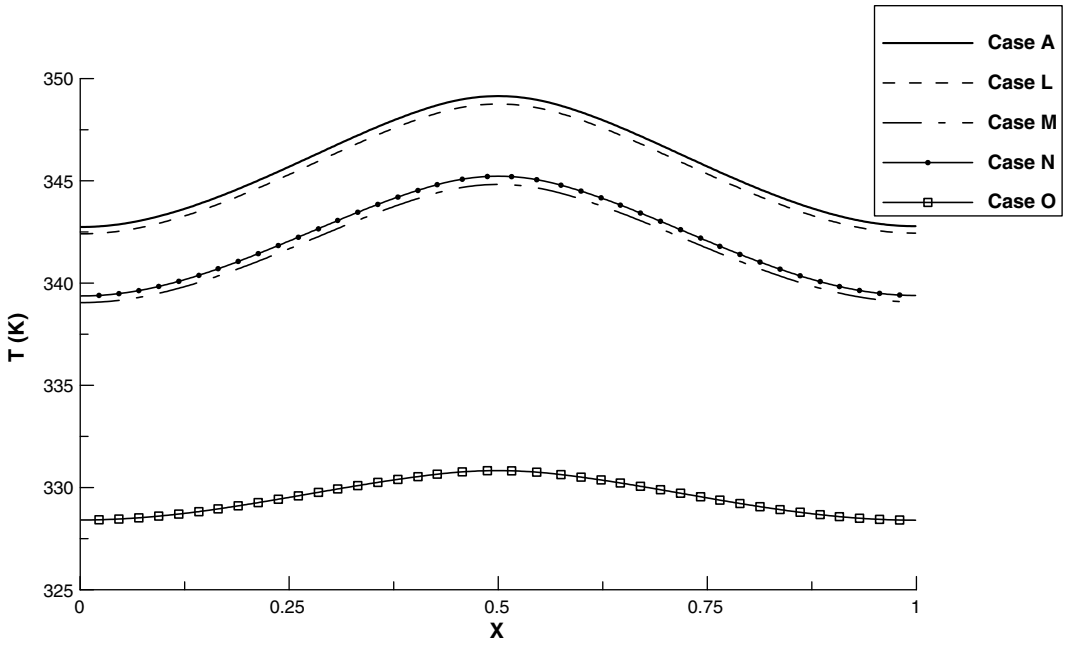

Fig. 10. The effects of thermal grease type and thickness on the temperature distribution at the silicon–glass interface at $t = 0.02$ s.

the literature data, the cycle time of 0.375 and 0.665 s are achieved, respectively.

5.8. Optimized PCR design

Based on a comprehensive investigation, case P is established as an optimum design for the PCR operation. Compared to base case A, the optimum design is achieved by increasing the inlet channel thickness and decreasing the exit channel thickness, velocity and flow rate, and the conductive plate thickness (Tables 1 and 2). To reduce the pressure drop, the maximum thickness of porous matrix in the optimized case is decreased such that it will result in the same inclination angle as the base case. The optimization results in a high temperature ramp (150.82 °C/s), low pumping power (12.36 W), and a uniform temperature distribution at the silicon–glass interface. To demonstrate that further changes in the geometry or properties of the PCR design do not result in any additional improvements, many additional cases were systematically analyzed. Case P was established as the optimum design as a result of these investigations.

6. Conclusions

An innovative and comprehensive methodology for rapid thermal cycling utilizing porous inserts was presented for maintaining a uniform temperature within a PCR microchip consisting of all the pertinent layers. An optimized PCR design which is widely used in molecular biology is presented for accommodating rapid transient and steady cyclic thermal management applications. Compared to what is available in the literature, the presented PCR design has a considerably higher heating/cooling temperature ramps and lower required power while resulting in a very uniform temperature distribution at the substrate at each time step. A comprehensive investigation of various pertinent parameters on physical attributes of the PCR system was presented. All pertinent parameters were considered simultaneously leading to an optimized design.

Acknowledgement

Awards through Grant Numbers B570317, B570318 and B563131 from Lawrence Livermore National Laboratory is gratefully acknowledged and appreciated.

References

[1] D.S. Lee, C.Y. Tsai, W.H. Yuan, P.J. Chen, P.H. Chen, A new thermal cycling mechanism for effective polymerase chain reaction in microliter volumes, Microsyst. Technol. 10 (2004) 579–584.
[2] D.S. Yoon, Y.S. Lee, Y. Lee, H.J. Cho, S.W. Sung, K.W. Oh, J. Cha, G. Lim, Precise temperature control and rapid thermal cycling in a micromachined DNA polymerase chain reaction chip, J. Micromech. Microeng. 12 (2002) 813–823.
[3] M.H. Hofmann, A. Akkoyuna, R. Flynn, A. Mathewson, H. Berney, M.M. Sheehan, Development of PCR conditions in a silicon microreactor DNA-amplification device, Int. J. Environ. Anal. Chem. 84 (11) (2004) 821–833.
[4] Z.Q. Niu, W.Y. Chen, S.Y. Shao, X.Y. Jia, W.P. Zhang, DNA amplification on a PDMS–glass hybrid microchip, J. Micromech. Microeng. 16 (2006) 425–433.
[5] M.A. Northrup, M.T. Ching, R.M. White, R.T. Watson, A mems-based miniature DNA analysis system, in transducers 93, in: Seventh International Conference on Solid State Sensors and Actuators, June 7–10, 1993, Yokohama Japan, pp. 924–926.
[6] H. Swerdlow, B.J. Jones, C.T. Wittwer, Fully automated DNA reaction and analysis in a fluidic capillary instrument, Anal. Chem. 69 (5) (1997) 848–855.

[7] A.F.R. Huhmer, J.P. Landers, Noncontact infrared-mediated thermocycling for effective polymerase chain reaction amplification of DNA in nanoliter volumes, Anal. Chem. 72 (21) (2000) 5507–5512.
[8] T. Ohashi, H. Kuyama, N. Hanafusa, Y. Togawa, A simple device using magnetic transportation for droplet-based PCR, Biomed. Microdevices (2007).
[9] E.T. Lagallya, P.C. Simpson, R.A. Mathies, Monolithic integrated microfluidic DNA amplification and capillary electrophoresis analysis system, Sensor. Actuat. B 63 (2000) 138–146.
[10] P. Wilding, M.A. Shoffner, L.J. Kricka, PCR in a silicon microstructure, Clin. Chem. 40 (9) (1994) 1815–1818.
[11] J. Singh, M. Ekaputri, PCR thermal management in an integrated Lab on chip, J. Phys.: Conferen. Series 34 (2006) 222–227.
[12] K. Shen, X. Chen, M. Guo, J. Cheng, A microchip-based PCR device using flexible printed circuit technology, Sensor. Actuat. B 105 (2005) 251–258.
[13] W.H. Grover, A.M. Skelley, C.N. Liu, E.T. Lagally, R.A. Mathies, Monolithic membrane valves and diaphragm pumps for practical large-scale integration into glass microfluidic devices, Sensor. Actuat. B 89 (2003) 315–323.
[14] C. Zhang, D. Xing, Miniaturized PCR chips for nucleic acid amplification and analysis: latest advances and future trends, Nucl. Acids Res. (2007) 1–15.
[15] E.K. Wheeler, W. Benett, P. Stratton, J. Richards, A. Chen, A. Christian, K.D. Ness, J. Ortega, L.G. Li, T.H. Weisgraber, K. Goodson, F. Milanovich, Convectively driven polymerase chain reaction thermal cycler, Anal. Chem. 76 (14) (2004) 4011–4016.
[16] J. Cheng, M.A. Shoffner, G.E. Hvichia, L.J. Kricka, P. Wilding, Chip PCR. II. investigation of different PCR amplification systems in microfabricated silicon–glass chips, Nucl. Acids Res. 24 (2) (1996) 380–385.
[17] K.D. Ness, E.K Wheeler, W. Benett, P. Stratton, A. Christian, A. Chen, J. Ortega, T.H. Weisgrabber, K.E. Goodson, Buoyancy-driven polymerase chain reaction (PCR) devices, Lawrence Livermore National Lab report, 2004.
[18] N.R. Beer, B.J. Hindson, E.K. Wheeler, S.B. Hall, K.A. Rose, I.M. Kennedy, B.W. Colston, On-chip, real-time, single-copy polymerase chain reaction in picoliter droplets, Anal. Chem. 79 (2007) 8471–8475.
[19] N. Park, S. Kim, J.H. Hahn, Cylindrical compact thermal-cycling device for continuous-flow polymerase chain reaction, Anal. Chem. 75 (2003) 6029–6033.
[20] M. Hashimoto, P.C. Chen, M.W. Mitchell, D.E. Nikitopoulos, S.A. Soper, M.C. Murphy, Rapid PCR in a continuous flow device, Lab on a chip, Roy. Soc. Chem. 4 (2004) 638–645.
[21] C.F. Chou, R. Changrani, P. Roberts, D. Sadler, J. Burdon, F. Zenhausern, S. Lin, A. Mulholland, N. Swami, R. Terbrueggen, A miniaturized cyclic PCR device – modeling and experiments, Microelectron. Eng. 61 (2002) 921–925.
[22] Q. Zhang, W. Wang, H. Hongshen, Y. Wang, Temperature analysis of continuous-flow micro-PCR based on FEA, Sensor. Actuat. B: Chem. 82 (1) (2002) 75–81.
[23] M.U. Kopp, A.J. Mello, A. Manz, Chemical amplification: continuous-flow PCR on a chip, J. Sci. 280 (5366) (1998) 1046–1048.
[24] J. Khandurina, T.E. McKnight, S.C. Jacobson, L.C. Waters, R.S. Foote, J.M. Ramsey, Integrated system for rapid PCR-based DNA analysis in microfluidic devices, Anal. Chem. 72 (13) (2000) 2995–3000.
[25] E.T. Lagally, I. Medintz, R.A. Mathies, Single-molecule DNA amplification and analysis in an integrated microfluidic device, Anal. Chem. 73 (3) (2001) 565–570.
[26] T.M.H. Lee, I.M. Hsing, A.I.K. Lao, M.C. Carles, A miniaturized DNA amplifier: its application in traditional chinese medicine, Anal. Chem. 72 (17) (2000) 4242–4247.
[27] E.T. Lagally, C.A. Emrich, R.A. Mathies, Fully integrated PCR-capillary electrophoresis microsystem for DNA analysis, Lab on a chip, Roy. Soc. Chem. 1 (2001) 102–107.
[28] S. Bhattacharya, Y. Gao, V. Korampally, M.T. Othman, S.A. Grant, S.B. Kleiboeker, K. Gangopadhyay, S. Gangopadhyay, Optimization of design and fabrication processes for realization of a PDMS-SOG-silicon DNA amplification chip, J. Micro-electromech. Syst. 16 (2) (2007).
[29] J.H. Daniel, S. Iqbal, R.B. Millington, D.F. Moore, C.R. Lowe, D.L. Leslie, M.A. Lee, M.J. Pearce, Silicon microchambers for DNA amplification, Sensor. Actuat. A 71 (1998) 81–88.
[30] S. Poser, T. Schulz, U. Dillner, V. Baier, J.M. Kohler, D. Schimkat, G. Mayer, A. Siebert, Chip elements for fast thermocycling, Sensor. Actuat. A: Phys. 62 (1–3) (1997) 672–675.
[31] P. Neuzil, C. Zhang, J. Pipper, S. Oh, L. Zhuo, Ultra fast miniaturized real-time PCR: 40 cycles in less than six minutes, Nucl. Acids Res. 34 (11) (2006).
[32] K. Vafai, S. Kim, Analysis of surface enhancement by a porous substrate, ASME J. Heat Transfer 112 (1990) 700–706.
[33] K. Vafai, P.C. Huang, Analysis of heat transfer regulation and modification employing intermittently emplaced porous cavities, ASME J. Heat Transfer 116 (1994) 604–613.
[34] A.R. Khaled, K. Vafai, The role of porous media in modeling flow and heat transfer in biological tissues, Int. J. Heat Mass Transfer 46 (2003) 4989–5003.
[35] K. Khanafer, K. Vafai, The role of porous media in biomedical engineering as related to magnetic resonance imaging and drug delivery, Heat Mass Transfer 42 (2006) 939–953.
[36] A.R. Khaled, K. Vafai, Heat transfer and hydromagnetic control of flow exit conditions inside oscillatory squeezed thin films, Numer. Heat Transfer J., Part A 43 (2003) 239–258.
[37] K. Khanafer, K. Vafai, Isothermal surface production and regulation for high heat flux applications utilizing porous inserts, Int. J. Heat Mass Transfer 44 (2001) 2933–2947.
[38] N. Zhu, K. Vafai, The effects of liquid–vapor coupling and non-Darcian transport on asymmetrical disk-shaped heat pipes, Int. J.Heat Mass Transfer 39 (1996) 2095–2113.
[39] Y. Wang, K. Vafai, An experimental investigation of the thermal performance of an asymmetrical flat plate heat pipe, Int. J. Heat Mass Transfer 43 (2000) 2657–2668.
[40] D.Y. Lee, K. Vafai, Comparative analysis of jet impingement and microchannel cooling for high heat flux applications, Int. J. Heat Mass Transfer 42 (1999) 1555–1568.
[41] K. Vafai, L. Zhu, Analysis of a two layered microchannel heat sink concept in electronic cooling, Int. J. Heat Mass Transfer 42 (1999) 2287–2297.
[42] K. Vafai, C.L. Tien, Boundary and inertia effects on flow and heat transfer in porous media, Int. J. Heat Mass Transfer 24 (1981) 195–203.
[43] FLUENT 6.3 users's guide, Lebanon US, 2006.
[44] K. Vafai, S. Kim, Forced convection in a channel filled with porous medium – an exact solution, ASME J. Heat Transfer 111 (1989) 1103–1106.